Polyvalent Glycomimetic-Gold Nanoparticle Conjugates reveal effects of glycan display on Multivalent Lectin-Glycan Interactions

Xinyu Ning,[†‡] Darshita Budhadev,[†‡] Sara Pollastri[#] Inga Nehlmeier,[‡] Amy Kempf,[‡] Iain Manfield,[ϕ] W. Bruce Turnbull,[†] Stefan Pöhlmann[‡,$] Anna Bernardi,[#] Xin Li,[ⱷ] Yuan Guo[ϱ,*], and Dejian Zhou[†,*]

[†] School of Chemistry and Astbury Centre for Structural Molecular Biology, University of Leeds, Leeds LS2 9JT, United Kingdom.

[#] Dipartimento di Chimica, Universita` degli Studi di Milano, via Golgi 19, Milano, Italy.

[‡] Infection Biology Unit, German Primate Center – Leibniz Institute for Primate Research, 37077 Göttingen, Germany.

[$] Faculty of Biology and Psychology, University of Göttingen, 37073 Göttingen, Germany.

[ϱ] School of Food Science & Nutrition and Astbury Centre for Structural Molecular Biology, University of Leeds, Leeds LS2 9JT, United Kingdom.

[ⱷ] Sphere Fluidics Ltd., Building One, Granta Centre, Granta Park, Great Abington, Cambridge, England, CB21 6AL, United Kingdom.

[ϕ] School of Molecular and Cellular Biology and Astbury Centre for Structural Molecular Biology, University of Leeds, Leeds LS2 9JT, United Kingdom.

[‡] These authors contributed equally to this work.

KEYWORDS. Gold nanoparticle, glycoconjugate, multivalent lectin-glycan interaction, glycomimetic, fluorescence quenching, binding thermodynamics, virus inhibition.

ABSTRACT: Multivalent lectin-glycan interactions (MLGIs) are widespread and vital for biology, making them attractive therapeutic targets. Unfortunately, the structural and biophysical mechanisms of several key MLGIs remain poorly understood, limiting our ability to design spatially matched glycoconjugates as potent therapeutics against targeting MLGIs. A synthetic pseudo-dimannose (psDiMan) ligand has been shown to selectively bind to a dendritic cell surface tetrameric lectin, DC-SIGN, over some other multimeric lectins sharing monovalent mannose specificity but having distinct cellular functions. Herein, we display psDiMan polyvalently onto gold nanoparticles (GNP-psDiMan) to probe how scaffold size and glycan valency control their multivalent binding properties with DC-SIGN. We reveal that GNP-psDiMan binds strongly, with sub-nM K_ds, to DC-SIGN and their binding affinity is enhanced with the increasing GNP scaffold size. Interestingly, there is a minimal, GNP size-dependent, glycan density threshold for forming strong MLGIs with DC-SIGN. Moreover, we have developed a new fluorescence quenching method for probing MLGI thermodynamics by quantifying MLGI affinities under varying temperatures in combination with the Van't Hoff analysis. We reveal that DC-SIGN binding with GNP-psDiMans is enthalpy driven, with the standard binding enthalpy changes (ΔH^0s) of ~ -100 kJ/mol, matching well to those measured by isothermal titration calorimetry. Such ΔH^0 values are ~4 folds that of the corresponding monovalent psDiMan-DC-SIGN binding, implying that all 4 binding sites in DC-SIGN are engaged in binding to GNP-psDiMan. Dynamic light scattering studies further show that DC-SIGN binds glycans from the same GNP-psDiMan. Finally, using particles pseudotyped with the Ebola virus glycoprotein, we show that GNP-psDiMans potently inhibit DC-SIGN-dependent augmentation of Ebola virus cellular entry with sub-nM level EC_{50} values. Interestingly, such EC_{50} values are comparable to their DC-SIGN binding affinities measured by fluorescence quenching in solution. These results indicate that GNP based fluorescence quenching is a versatile method to reveal MLGI thermodynamics and binding determinants of high affinity MLGI interactions, and to predict GNP-glycan antiviral properties.

Introduction

Multivalent lectin-glycan interactions (MLGIs) are widespread and vital for many important biological events, such as infection, cell-cell communication, and the regulation of immune response.[1-6] For example, pathogens often employ specific glycan patterns to target host cell lectin receptors (or vice versa) to initiate contact and infection, while immune cells often employ lectins to recognize specific pathogen-associated glycan patterns to differentiate pathogens and to instruct immune responses.[4-10] Therefore, it is unsurprising that constructing glycan structures to target specific MLGIs has been a very active and attractive therapeutic approach against a wide range of viral infections, cancer, and other immune dysregulation diseases.[1-5, 11-18] Strategies employed often include the design of monovalent glycans against specific structures of individual carbohydrate-recognition-domains (CRDs) and displaying glycans multi-/poly- valently onto various nanoscale scaffolds.[1-2, 11-26] This is mainly because most monovalent glycan-CRD interactions are too weak to produce high enough therapeutical effects. Displaying multiple glycans on a suitable scaffold to create a perfect spatial and orientation match to the target lectin's multiple CRDs will greatly enhance not only their binding affinity but also specificity.[11, 25] The latter is of great importance for potential applications *in vivo* due to the overlapping glycan specificity, at the monovalent levels, of various multimeric lectins.[4]

A wide variety of nanostructures, e.g., polymers, dendrimers, liposomes, polymersomes, proteins, and inorganic nanoparticles, have been employed as scaffolds to construct multi-/poly- valent glycoconjugates to enhance their MLGI

affinity and specificity with target lectins.[1-3, 11-17, 19-28] The biophysical parameters of binding to target lectins are mainly evaluated by conventional biophysical techniques, such as surface plasmon resonance (SPR), [29] and isothermal titration calorimetry (ITC). [30-31] While these traditional biophysical methods are powerful in obtaining quantitative binding affinity, kinetic, and thermodynamic data, they cannot provide key structural information, e.g., binding site organization, binding mode, and inter-binding site distances etc., which are of critical importance for designing spatial matched glycoconjugates against a particular MLGI for therapeutic interventions. In addition, each of these techniques also suffers from their own limitations. For example, while ITC can provide accurate measure of binding enthalpy changes (ΔHs), it cannot provide accurate binding affinities for very strong interactions with low- to sub- nM K_ds. [32-33] Whereas SPR measures binding interactions happening on surfaces, which is a very different environment from that happening in solution. As a result, the binding kinetic and thermodynamic data obtained in SPR may not reflect what happens in solution.[28] Moreover, most previous studies have employed nanoparticles only as passive scaffolds to display polyvalent glycans to enhance MLGI affinity and/or specificity,[1-3, 12-13] however, the unique, size-dependent optical properties of nanoparticles, which are fundamental and critically important for nanomaterials, were not exploited as readout signals for MLGI affinity quantitation.

To address the above stated limitations, we have recently demonstrated that small nanoparticles (e.g., ~4 nm CdSe/ZnS quantum dots, QDs,[20, 27-28] and a ~5 nm gold nanoparticle, GNP,[14]) densely glycosylated with fragments of the natural high mannose structures are powerful probes for MLGIs. By harnessing the unique, size-dependent strong fluorescence (for QDs), or fluorescence quenching (for GNPs) properties, we have developed a robust, sensitive method for MLGI affinity quantitation based on the Förster resonance energy transfer (FRET, with QD) or fluorescence quenching (with GNP).[14, 20] We have further dissected the exact binding modes of the target MLGIs by analyzing the hydrodynamic size and capturing binding induced nanoparticle-lectin assemblies under their native dispersion state by exploiting the nanoparticle's size and high contrast under transmission electron microscopy (TEM) imaging.[14, 20] Using a pair of critically important, closely related tetrameric lectin viral receptors, DC-SIGN[34] and DC-SIGNR[35], as model lectins, we have revealed that each DC-SIGN binds simultaneously to one nanoparticle-glycan via all four of its CRDs, giving rise to isolated nanoparticle-lectin assemblies and strong affinities (low to sub-nM K_ds). In contrast, DC-SIGNR crosslinks with multiple nanoparticle-glycans, resulting in extended large-scale nanoparticle-lectin assemblies and markedly weaker affinities in binding to nanoparticle-glycans than DC-SIGN.[14, 20] Moreover, we have found that nanoparticle-glycans only potently and robustly block DC-SIGN-, but not DC-SIGNR-, mediated augmentation of Ebola virus cell entry, and thus demonstrating the critical role of the MLGI binding mode in the ability of glycoconjugates to block viral infections.[14]

Despite these advances, how nanoparticle scaffold size as well as glycan type and density control MLGI affinity and other key biophysical parameters remains to be explored. Here, a synthetic glycomimetic, a pseudo-α-1,2-mannobioside (psDiMan) that shows a different binding mode on DC-SIGN CRD from the natural high mannose fragment counterpart, α-manno-α-1,2-biose (DiMan),[36-38] has been displayed polyvalently onto two different sized GNP scaffolds (e.g., ~5 and ~13 nm in diameter, abbreviated as G5-psDiMan and G13-psDiMan, respectively) under systematically varying densities. psDiMan is designed by replacing the reducing end mannose of DiMan with a cyclohexanediol scaffold locked in a diaxial conformation by two carbomethoxy groups (**Figure 1**).[39] The cyclohexane framework was found to offer specific hydrophobic interactions with Val351 in DC-SIGN, resulting in moderate selectivity towards DC-SIGN CRD over that of langerin, despite their sharing glycan specificity.[36] We have quantified Gx-psDiMan-DC-SIGN (x=5 or 13) binding affinities, *via* GNP's strong fluorescence quenching properties,[40-43] and demonstrated that there is a minimal, GNP size-dependent, glycan density threshold in order to form strong MLGI with DC-SIGN. We have then applied the Van't Hoff analysis of their temperature dependent MLGI affinities and revealed that DC-SIGN binding with Gx-psDiMan (for both x = 5 and 13) is enthalpy driven and the binding thermodynamic parameters derived from fluorescence quenching match well to those obtained from ITC. Moreover, we have found that their MLGI enthalpy changes (ΔHs) are ~4 times that of monovalent binding, suggesting that all 4 CRDs in each DC-SIGN are engaged in binding. Finally, by employing particles pseudotyped with the glycoprotein (GP) of Ebola virus ($EBOV_{pp}$), we have investigated the ability of Gx-psDiMan to block DC-SIGN-promoted cell entry of EBOV-GP_{pp}.[14, 20] We reveal that Gx-psDiMan can potently block viral entry to host cells, and their antiviral potencies are positively correlated to their DC-SIGN binding affinity measured by fluorescence quenching. Together, these results have established Gx-psDiMan as a powerful new biophysical probe for MLGI affinity enhancing mechanisms, which can also serve as potent antiviral agents.

Results and Discussion

1. Preparation and characterisation of essential materials.

1.1 Design and synthesis of LA-EG_n-based ligands. A lipoic acid-tetra(ethylene glycol) based multifunctional glycan ligand, LA-EG_4-psDiMan, was designed (**Scheme 1**). It contains three functional domains, a LA group for strong anchoring on the GNP surface by forming two strong Au-S bonds;[14, 44] a flexible tetra(ethylene glycol) linker to afford the terminal glycan with some flexibility and impose high water solubility, stability, and resisting non-specific interactions;[45-46] and a terminal pseudo-α-1,2-mannobioside (psDiMan) for specific DC-SIGN binding.[36] Besides, a LA-EG_2 ligand containing an EG_2-OH terminal group, abbreviated as LA-EG_2-EG_2-OH, was also designed as an inert spacer ligand to tailor the GNP surface glycan density (see **Fig. 1**). Self-assembled monolayers terminated with oligo(ethylene glycol) groups are well-known for their ability to resist non-specific adsorptions and interactions of biomolecules.[45, 47]

Both ligands contain the same LA based GNP surface anchoring group with the same overall EG linker length, therefore, they should have the same GNP anchoring and surface display properties. This allows us to readily tune GNP surface glycan density by simply varying the glycan: spacer ligand ratio (but with a fixed total ligand: GNP ratio) used in the GNP-glycan preparation.

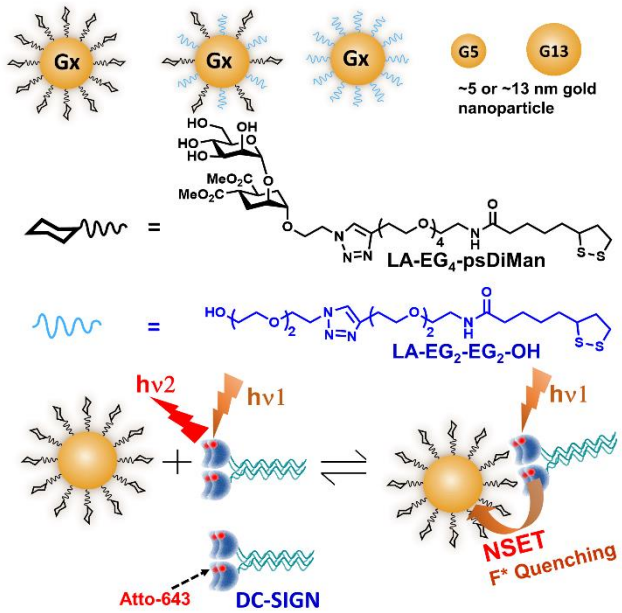

Fig. 1. (**A**) Schematic shows of Gx-psDiMan with varying glycan density and GNP scaffold size. The chemical structures of the psDiMan and spacer ligands are also shown. (**B**) A schematic show of the principle of the GNP-based fluorescence quenching assay. Upon binding, the Atto-643 fluorescence is efficiently quenched by GNP in proximity *via* nano surface energy transfer (NSET).

The LA-EG_4-psDiMan glycan and LA-EG_2-EG_2-OH spacer ligands were synthesized via the route shown schematically in **Scheme 1**. Briefly, lipoic acid was first coupled to the commercial H_2N-EG_n-C≡CH (n = 2 or 4) *via* dicyclohexylcarbodiimide/4-N,N-dimethylaminopyridine mediated amide coupling to give LA-EG_n-C≡CH in good yields, e.g., 72% for n = 2, and 85% for n = 4.[14, 48] psDiMan appending an α-$(CH_2)_2$-N_3 linker in the pseudo-anomeric position (psDiMan-C_2-N_3) was synthesized as described previously.[49] Finally, LA-EG_n-C≡CH was coupled to psDiMan-$(CH_2)_2$-N_3 (n = 4) or HO-EG_2-N_3 (n = 2) *via* the copper-catalyzed click reaction in the presence of $CuSO_4$, sodium ascorbate (for reducing Cu^{2+} to Cu^{+}) and tris(benzyltriazolylmethyl)amine (for stabilizing the formed Cu^{+} catalyst) and purified by size exclusion chromatography using a Biogel P2 column *via* our established protocols[14, 48] to give the desired LA-EG_4-psDiMan or LA-EG_2-EG_2-OH ligand in ~80% or 85% yields, respectively. Their chemical structures were confirmed by $^1H/^{13}C$ NMR and LC-MS spectra (supporting Information, **SI**, **Figs. S1 and S2**).

1.2. Preparation and characterisation of Gx-psDiMan. Two different sized GNPs, with diameters of ~5 and ~13 nm (denoted as G5 and G13), respectively, were prepared by citrate reduction of $H[AuCl_4]$ in the absence (for G13) or presence of a small amount of tannic acid (for G5) by following the literature methods,[50-52] and their core sizes were confirmed by TEM (**SI, Fig. S3**). They were then incubated with the LA-EG_4-psDiMan ligand in an aqueous solution under a total ligand: GNP molar ratio of 1000 and 3000 for G5 and G13, respectively, to prepare the desired Gx-psDiMan conjugates (x = 5 or 13). We have found previously that treating G5 with 1000 molar equivalent of LA-EG_n-glycan ligand produced highly stable and densely glycosylated G5-glycans.[14] Here, a higher ligand: GNP molar ratio of 3000:1, about 2.4 times the ligand ratio required to coat G13 with a self-assembled monolayer of LA-EG_n-ligand was used, ensuring that the G13 was fully coated with the desired glycan ligands (see **SI, section 2.3**). To investigate how GNP surface glycan density affect their MLGI properties with DC-DIGN, the GNPs were further incubated with mixed the LA-EG_4-psDiMan and LA-EG_2-EG_2-OH ligands of varying ratios (but under a fixed total ligand: GNP ratio as above). In this way, a serial of Gx-psDiMan conjugates with the psDiMan content being systematically varied from 0, 6.3, 12.5, 25, 50, 75 to 100% were prepared (see **Table 1**). Each LA-based ligand can form 2 Au-S bonds on binding onto the GNP surface, with a total bond enthalpy comparable to a typical covalent C-C single bond (~90 *vs.* ~83 kcal.mol^{-1}).[53] As a result, the LA-based ligands are expected to be non-mobile after self-assembly on the GNP surface. Thus, the LA-glycan and LA-spacer ligands should be randomly distributed on GNP surface without phase separation.

Scheme 1. Synthetic route to the LA-EG_4-psDiMan and LA-EG_2-EG_2-OH ligands.

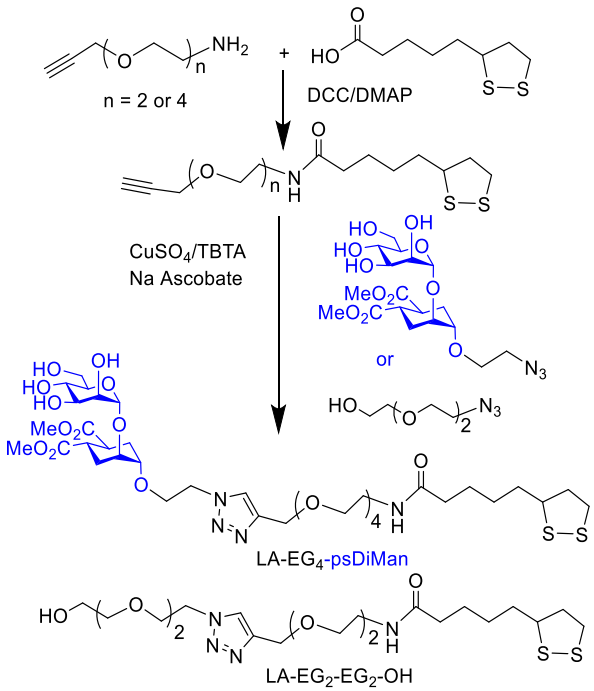

Table 1. Summary of key parameters of Gx-psDiMan conjugates under different glycan densities. D_h = hydrodynamic diameter (mean ± ½ FWHM); N = glycan valency per GNP (assuming identical GNP binding properties for LA-EG_4-psDiMan and LA-EG_2-EG_2-OH); X = average inter-glycan distance. Apparent K_d and n values were obtained from fitting the QE -concentration plots by equation 2 with fixed QE_{max}% = 100 (R^2 > 0.995 for all fits); "–" indicates binding curves not fitted, due to binding being too weak; multivalent binding enhancement factor, $\beta = K_d^{mono}/K_d$, where K_d^{mono} = 1.1 mM, obtained from ITC (see **SI**, **Fig. S9)**.

Gx	psDiMan(%)	D_h (nm)	N	Inter-glycan distance, X (nm)	Apparent K_d (nM)	Hill coefficient, n	β	β/N
G5	0	12.9 ± 2.4	0	-	-	-	-	-
	6.3	9.3 ± 2.4	30 ± 3	3.4 ± 0.2	-	-	-	-
	12.5	9.6 ± 2.1	60 ± 5	2.5 ± 0.1	-	-	-	-
	25	11.8 ± 2.5	119 ± 11	2.2 ± 0.1	2.74 ± 0.24	0.47 ± 0.02	400,000	3,400
	50	11.8 ± 2.4	238 ± 22	1.53 ± 0.07	1.38 ± 0.26	0.54 ± 0.04	800,000	3,300
	75	12.9 ± 2.2	357 ± 32	1.37 ± 0.06	0.68 ± 0.07	0.46 ± 0.07	1,600,000	4,500
	100	11.4 ± 2.3	476 ± 43	1.05 ± 0.05	0.22 ± 0.05	0.37 ± 0.02	5,000,000	10,500
G13	0	16.7 ± 3.2	0	-	-	-	-	-
	6.3	18.1 ± 2.8	124 ± 12	3.3 ± 0.2	11.5 ± 0.4	0.74 ± 0.02	96,000	770
	12.5	19.5 ± 3.3	245 ± 23	2.5 ± 0.1	0.55 ± 0.03	0.54 ± 0.02	2,000,000	8,200
	25	18.1 ± 2.9	491 ± 47	1.6 ± 0.1	0.30 ± 0.02	0.57 ± 0.03	3,700,000	7,500
	50	18.9 ± 3.7	982 ± 93	1.21 ± 0.06	0.13 ± 0.02	0.55 ± 0.04	8,500,000	8,700
	75	18.2 ± 3.0	1472 ± 140	0.95 ± 0.04	0.15 ± 0.02	0.47 ± 0.02	6,700,000	4,500
	100	18.4 ± 3.6	1963 ± 186	0.83 ± 0.04	0.21 ± 0.02	0.59 ± 0.02	5,200,000	2,700

The successful preparation of Gx-psDiMan conjugates was supported by a small increase of the hydrodynamic diameters (D_hs) compared to the parent, citrate stabilized Gxs and the formation of monodispersed particles in water with narrow size distributions of hydrodynamic diameters (D_hs, see **Table 1** and **SI, Fig. S4)**. The resulting Gx-psDiMan conjugates were found to be highly stable, no visible changes of solution color or precipitation were observed after storage for > 6 months. No changes in UV-vis absorption spectra after dispersion to a standard DC-SIGN binding buffer (20 mM HEPES, 100 mM NaCl, 10 mM $CaCl_2$, pH7.8). The concentrations of Gx-psDiMan were estimated from their maximal absorbance at ~515 (for G5) and ~520 nm (for G13) using an extinction coefficient of 6.3 ×10^6 (for G5) and 2.32 × 10^8 M^{-1} cm^{-1} (for G13), respectively.[14, 51]

The glycan valency on Gx surface was estimated from the difference in glycan ligand amount between that added and that remained unbound in the post-incubation supernatant via a phenol-sulfuric acid carbohydrate quantifying method as described previously (**SI, Fig. S5)**,[14, 20, 54] and the results were summarized in **Table 1.** By using the hydrodynamic diameter and glycan valency of Gx-psDiMan conjugates under different glycan content, the average glycan footprint, deflection angle, and inter-glycan distance were estimated *via* the method reported by the Mirkin group,[55] and summarized in **Table 1** and **SI, Table S1**. A systematically increasing glycan footprint, deflection angle, and inter-glycan distance were obtained with the decreasing glycan content on the Gx surface. Interestingly, the average inter-glycan distances for G5-psDiMan100% (~1.05 nm) and G13-psDiMan (50-100%, ~0.8-1.2 nm) are comparable to the majority of inter-glycan sequon distances (~0.7-1.3 nm) found on gp160,[56] the HIV surface heavily glycosylated trimeric glycoprotein, which mediates specific DC-SIGN binding and viral infection.

1.3. Protein production and labelling with Atto-643. DC-SIGN forms stable homotetramers on cell surface, mediated by the neck region coiled-coil formation. We and others have demonstrated previously that DC-SIGN extracellular domain faithfully maintains the tetramer structure and MLGI properties of the full-length protein.[27, 57] Hence, DC-SIGN extracellular segment (named as DC-SIGN hereafter) was used to study its MLGI properties with Gx-psDiMan in solution. To facilitate sensitive fluorescence based binding detection, the recombinant DC-SIGN mutant DC-SIGN-Q274C was expressed in E. coli and purified using Sepharose-Mannose affinity chromatography as described previously.[14, 27] The purified proteins were site specifically labelled with a maleimide modified Atto-643 dye (named as labelled DC-SIGN) through the Michael addition between thiol and maleimide as described previously.[14, 20] This labelling site is close to, but not sits in the CRD's glycan binding pocket,[37] and thus dye-labelling does not affect CRD's glycan binding properties as confirmed previously.[14, 20, 28] Atto-643 was chosen here due to its high fluorescence quantum yield, excellent photostability, and strong hydrophilicity, thereby minimizing any potential interfere with the CRD structure and glycan binding properties. Moreover, its fluorescence emission peaks at the far-red region of the visible spectrum (e.g., λ_{EX} = 630 nm, λ_{EM} ~660 nm), which can minimize the potential interference with fluorescence readout arising from the GNP's inner filter effect. The success of protein production and Atto-643 labelling were confirmed from their respective high resolution mass spectra (HRMS), where an increase of molecular mass of 935 was observed. Using the molecular mass peak areas of the labelled and unlabeled proteins, a labelling efficiency of ~92% per protein monomer was obtained **(SI, Fig. S6)**.

The recombinant wild-type DC-SIGN (no dye labeling) was also expressed and purified, to investigate DC-SIGN binding to Gx-psDiMan using dynamic light scattering (DLS) and ITC. Protein concentration was determined from its UV absorbance at 280 nm using an extinction coefficient of 2.82 × 10^5 M^{-1} cm^{-1} (tetramer) as reported previously.[20, 27]

2. Quantifying Gx-psDiMan-DC-SIGN MLGI affinity and thermodynamics via GNP based fluorescent quenching. To investigate how GNP size and glycan density affect their MLGI with DC-SIGN, we quantified their binding affinities using GNP's strong fluorescence quenching properties.[40-42] Here, varying concentrations of labelled DC-SIGN and Gx-psDiMan were mixed under a fixed mole ratio of 1:1 in a binding buffer (20 mM HEPES, 100 mM NaCl, 10 mM $CaCl_2$, pH 7.8) containing large excess of a non-target serum protein, bovine serum albumin (BSA, 1 mg/mL), which serves to minimize any nonspecific interactions.[14] It can also reduce nonspecific adsorption of proteins and/or Gx-psDiMans on surfaces, which can be a major source of experimental errors for assays performed at low concentrations (10 nM or below).[58] Moreover, serum proteins are of high abundance *in vivo*, therefore, this also makes the binding environments resemble more closely to real biological situations. The Gx-psDiMan and labelled DC-SIGN samples were incubated for 20 min at room temperature before their fluorescence spectra (from 650 to 800 nm) were recorded under a fixed λ_{EX} of 630 nm. Labelled DC-SIGN only samples (without Gx-psDiMan) were also recorded under identical conditions, which serve as controls to determine the quenching efficiency (QE) at each concentration (C) *via* equation (1):[14]

$$QE\% = \frac{IF_0 - IF}{IF_0} \times 100\% \qquad (1)$$

Where IF_0 and IF are the integrated fluorescence of labelled DC-SIGN in the absence and presence of 1 molar equivalent of Gx-psDiMan, respectively. GNP can efficiently quench a wide range of fluorophores *via* a nano surface energy transfer (NSET) mechanism (QE is proportional to the inverse 4th power of separation distance, d, i.e., $QE = 1/[1 + (d/d_0)^4]$,[42] where d_0 is the separation distance giving 50% quenching). Fluorescence quenching *via* the NSET mechanism is more effective and covers a greater distance range than organic quenchers based on the Förster resonance energy transfer (FRET, where QE is proportional to the inverse 6th power of dye-quencher distance, R, $QE = 1/[1 + (R/R_0)^6]$ mechanism.[41-42] Moreover, a GNP has been shown to quench fluorescence by up to 99.97% in a closed DNA hairpin structure.[40] Therefore, it is safe to assume that the measured QE% here represents the percentage of lectins that are bound to Gx-psDiMan. Thus, the apparent binding equilibrium dissociation constant (K_d) can be derived from the *QE-C* relationship by fitting with the Hill's equation (2): [14]

$$QE = \frac{QE_{max} \times C^n}{K_d^n + C^n} \qquad (2)$$

Where QE_{max}, K_d, C, and n are the maximum QE (fixed at 100%), apparent binding equilibrium dissociation constant, protein concentration, and Hill coefficient, respectively.

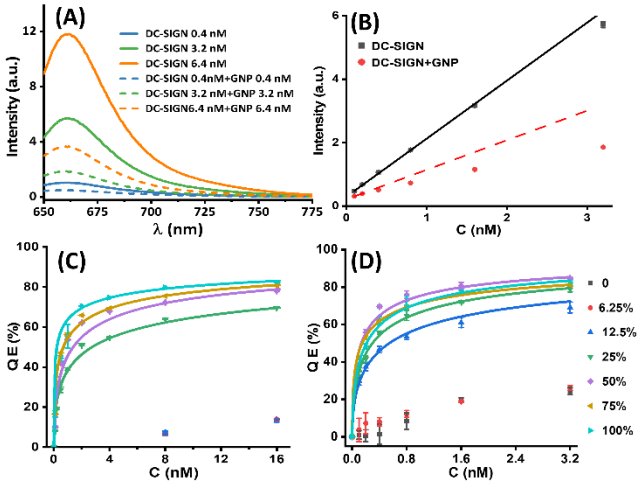

Fig. 2. (**A**) Fluorescence spectra of Atto-643 labelled DC-SIGN (varying concentrations) in the absence (solid lines) or presence (broken lines) of 1 molar equivalent of G13-psDiMan100%. (**B**) Integrated fluorescence intensity (IF) – concentration (C) plots for labelled DC-SIGN in the absence (black dots, with linear fit, R^2 = 0.995) and presence (red dots) of G13-psDiMan. (**C, D**) Plots of QE% *vs. C* for labelled DC-SIGN binding with 1 molar equivalent of G5-psDiMan (**C**) or G13-psDiMan (**D**) under a variety of glycan densities fitted by the Hill's equation (eq. 2).

The representative fluorescence spectra of labelled DC-SIGN before and after mixing with G13-psDiMan (100% glycan density) at 1:1 molar ratio under different Cs were shown in **Fig. 2A** (fluorescence spectra showing the binding of G5-psDiMan with labelled DC-SIGN were given in the **SI, Fig. S8**). It is apparent that labelled DC-SIGN fluorescence was greatly reduced in the presence of G13-psDiMan (or G5-psDiMan, **SI. Fig. S8**), especially at elevated concentrations. A plot of the integrated fluorescence (IF) *vs. C* (**Fig. 2B**) further revealed that, in the absence of G13-psDiMan, the fluorescence of labelled DC-SIGN alone increased linearly (R^2 >0.995) with the increasing C; while the presence of G13-psDiMan significantly and progressively quenched protein fluorescence, leading to the IF-C relationship to deviated more and more from linear (**Fig. 2B**). This result is fully consistent with that expected from that an increasing proportion of DC-SIGN are bound to G13-psDiMan and get quenched. The resulting QE - C relationships for DC-SIGN binding with G5-psDiMan and G13-psDiMan (with a variety of psDiMan contents) were obtained and fitted by the Hill's equation (eq. 2) as shown in **Figs. 2C** and **2D,** respectively. The detailed fitting parameters were summarized in **Table 1.** The relationships of the apparent K_d, MLGI enhancement factor (β, where $\beta = K_d^{mono}/K_d$, and K_d^{mono} = 1.1 mM obtained from ITC, see **SI, Fig. S9**) and per psDiMan normalized enhancement factor (β/N, where N is the psDiMan valency on

each GNP) as a function of psDiMan content (%) were shown in **Fig. 3A, 3A and 3C**, respectively.

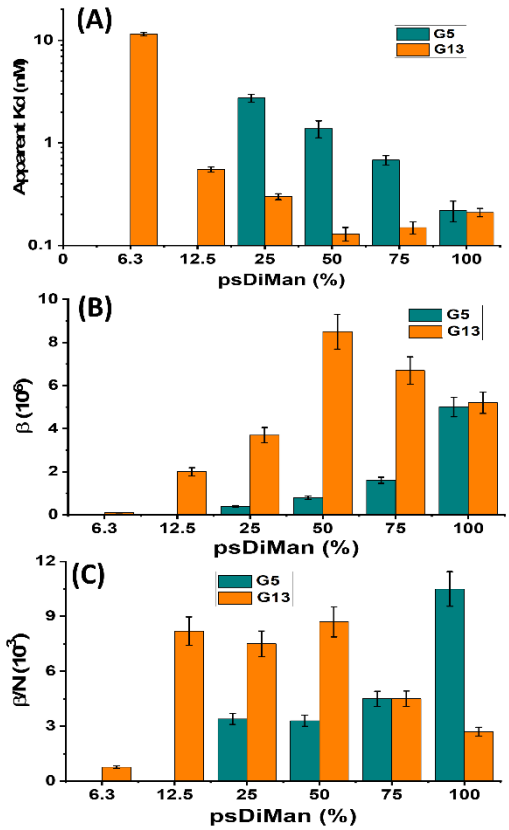

Fig. 3. (**A**) Apparent binding K_ds for DC-SIGN binding with Gx–psDiMan (x = 5, yellow; x = 13, blue) as a function of surface psDiMan content%; (**B**) plots of multivalent affinity enhancement factor (β) or (**C**) per psDiMan normalized affinity enhancement factor (β/N) for G5-psDiMan (blue) or G13- psDiMan (yellow) binding with labelled DC-SIGN as a functional of surface psDiMan content% obtained by fluorescence quenching assay (DC-SIGN affinities for G5-psDiMan at psDiMan contents of ≤12.5% were too weak to be measured accurately).

Based on the results of **Fig. 3 and Table 1**, four conclusions can be drawn. (1) There is a minimal, GNP size dependent, psDiMan content on its surface in order to form strong DC-SIGN binding (*i.e.,* sub- to low- nM K_ds). The thresholds are 25% and 12.5% for G5 and G13 (denoted as G5-psDiMan25% and G13-psDiMan12.5%), respectively. (2) Above this threshold, DC-SIGN binding affinity increased gradually with the increasing psDiMan content on G5 till reaching 100%. While that for G13-psDiMan, the trend was less clear: it gave the strongest DC-SIGN affinity with 50% psDiMan content (although the differences with those of 75 and 100% psDiMan are small and close to the assay detection limit), and further increasing or reducing psDiMan content led to slightly reduced affinity. (3) The highest DC-SIGN affinity was obtained with G13-psDiMan50%, which gave an impressively strong apparent binding K_d of ~0.13 nM. This affinity represents a massive, 8.5 million fold MLGI affinity enhancement ($\beta = K_d^{mono}/K_d^{MLGI}$) over that of the corresponding monovalent psDiMan-DC-SIGN binding (K_d^{mono}, determined as 1.1 mM by ITC, see **SI, Fig. S9**) and per glycan normalized enhancement factor, β/N, of ~8,700. This MLGI affinity is significantly stronger, by ~28 fold, than that of G5 coated with 100% LA-EG_2-EG_2-DiMan (*e.g.,* apparent K_d ~ 3.8 nM),[14] its equivalent DC-SIGN natural DiMan ligand of the same overall EG linker length, despite the fact that its monovalent affinity is slightly weaker than that of the latter (e.g., K_d^{mono} 1.1 mM *vs.* 0.9 mM,[59] both obtained from ITC, **SI, Fig. S9**). This result shows that displaying psDiMan polyvalently on a GNP surface is more effective in enhancing its MLGI affinity with DC-SIGN than that with DiMan, a natural glycan ligand for DC-SIGN, presumably due to their different binding motifs on DC-SIGN CRD.[36, 60] Therefore, we cannot directly use the relative strength of lectin-glycan monovalent affinity to predict their relative MLGI strengths involving polyvalent glycoconjugates. (4) The per psDiMan normalized enhancement factor, β/N, as a function of GNP surface psDiMan contents was found to depend strongly on the GNP size. For G5-psDiMan, its β/N generally increased with the increasing psDiMan content and reached the maximum at 100% psDiMan; under which it gave a highly impressive β/N value of ~10000. While for G13-psDiMan, its β/N broadly plateaued at ~8000 for psDiMan content between 12.5% and 50%, and further increasing the psDiMan content led to a markedly reduced β/N value (**Fig. 3C**). This result reveals a key role of surface curvature of glycoconjugate in their ability to form strong MLGI with DC-SIGN.

The difference in psDiMan density threshold for G5 and G13 -psDiMan to achieve strong MLGI with DC-SIGN can be rationalized from the assumption that strong MLGIs are only formed when all four CRDs in DC-SIGN are engaged in binding. While the detailed crystal structure of DC-SIGN tetramer remains unknown, results from our group as well as others indicate that all 4 binding sites in DC-SIGN point upwardly in the same direction, allowing them to bind simultaneously to multiple glycans on the same Gx surface.[14, 20, 27] This was also confirmed from the hydrodynamic diameter (D_h) measurement of Gx-psDiMan100% + DC-SIGN samples under a variety of DC-SIGN: Gx-psDiMan molar ratios, which revealed only a single D_h species for both G5- and G13-psDiMan binding with DC-SIGN. Their D_hs initially increased with the increasing DC-SIGN: Gx ratio, and then plateaued at a ratio of ~6:1 or ~32:1 for G5- or G13- psDiMan, respectively. This result indicates an increasing number of DC-SIGN molecules are bound to each Gx-psDiMan before surface binding saturation. Moreover, the saturated D_hs were found to be monodisperse and comparable to that expected for a central Gx-psDiMan particle coated with a monolayer of DC-SIGN molecules (~50-60 nm), implying that DC-SIGN must have bound to the central Gx-psDiMan particle with all four CRDs (**SI, Section 7, Figs. S11-S13**). Given that the terminal psDiMans are displayed on the Gx surface *via* a flexible EG_4 linker, it is reasonable to assume that any psDiMan groups within the projected footprint of each CRD on the Gx surface (~7 nm^2, based on a spherical CRD structure of ~3 nm in diameter),[37] could adapt and bind to that CRD. Therefore, any Gx-psDiMan conjugates with a glycan footprint

smaller than 7 nm^2 are expected to be able to bind to all four CRDs in DC-SIGN, giving rise to strong MLGI affinity. This result matches well to the drastic decrease of DC-SIGN MLGI affinity observed for G13-psDiMan as psDiMan content decreased from 12.5% to 6.3% (*i.e.*, average glycan footprint increased from ~4.9 to 9.4 nm^2, see **SI, Table S1**). The latter psDiMan content is below the threshold required to allow all four CRDs in DC-SIGN to engage in binding. For G5-psDiMan, a higher glycan content threshold is required to form tetravalent binding, presumably because of its larger surface curvature, giving rise to a glycan deflection angel being twice as big as that of its G13-psDiMan counterpart (e.g., 29.7 ± 1.3 ° *vs.* 14.6 ± 0.7° for G5- *vs.* G13-psDiMan12.5%, see SI, **Table S1**).

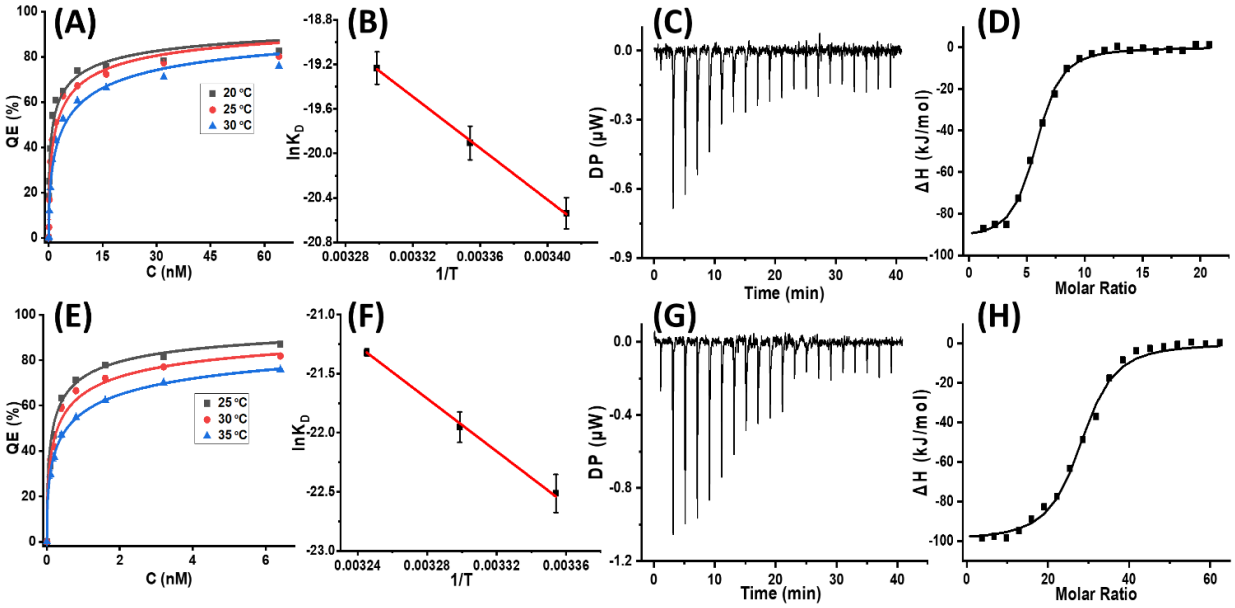

Fig. 4. The QE%-*C* relationships for DC-SIGN binding with G5-psDiMan100% (**A**) or G13-psDiMan100% (**E**) under three different temperatures fitted by Hill's equation, and the corresponding Van't Hoff plots (lnK_d *vs.* 1/T plots) for DC-SIGN binding with G5-psDiMan (**B**) or G13-psDiMan (**F**). ITC titration curves for DC-SIGN binding with G5-psDiMan100% (**C**) or G13-psDiMan100% (**G**) and their respective fitting curves (D, H).

3. Probing MLGI thermodynamics by GNP fluorescence quenching and comparing those obtained with ITC.

To extend the capacity of GNP fluorescence quenching assay in probing the binding thermodynamics of high affinity MLGIs, we also measured the binding K_ds between G5- or G13- psDiMan100% and labelled DC-SIGN under 3 different temperatures. Both of their quenching efficiencies (QEs) were found to decrease with the increasing temperature, indicating weakened interactions (larger K_ds values). We then applied the Van't Hoff analysis to derive their binding thermodynamics by combining the two Gibbs free energy equations (eqs. 3 and 4).[28] The changes of the standard binding enthalpy (ΔH^0) and entropy (ΔS^0) were obtained by taking a linear fit of the resulting ln(K_d) against the reciprocal of temperature, 1/T, *via* equation 5 (**Fig. 4**). The results obtained from the fittings were summarized in **Table 2**.

$$\Delta G^0 = RT ln K_d \qquad (3)$$

$$\Delta G^0 = \Delta H^0 - T\Delta S^0 \qquad (4)$$

$$ln\,(K_d) = \frac{\Delta H^0}{R}\frac{1}{T} - \frac{\Delta S^0}{R} \qquad (5)$$

Where R is the ideal gas constant, 8.314 J K^{-1} mol^{-1}.

In addition, we also measured the binding ΔH^0s between Gx-psDiMan and wild type DC-SIGN by isothermal titration calorimetry (ITC). These were performed by titrating concentrated DC-SIGN (30 μM) into concentrated Gx-psDiMan solution (e.g., 300 nM for x = 5, and 100 nM for x = 13) in the ITC cell to measure binding induced heat changes (see **SI, section 6**) and the results were summarized in **Table 2**. It should be noted that ITC cannot provide accurate measurement of the binding ΔG^0 (hence K_d) directly for very strong interactions (e.g., sub- to low- nM K_ds),[31, 33] although its measurement of ΔH^0 values is accurate.

As shown in **Table 2**, the binding ΔH^0 values obtained from the GNP fluorescent quenching assay agreed very well with those obtained by ITC, thereby confirming that our GNP based fluorescence quenching can be used as a reliable method to probe MLGI thermodynamic parameters. Specifically, both G5- and G13- psDiMan100% binding with DC-SIGN were found to be enthalpy driven, with comparable negative ΔH^0s of ~-95 KJ.mol^{-1} **(Table 2, Fig. 4)**. Interestingly, their multivalent binding ΔH^0s are about 4 time of that of psDiMan-DC-SIGN monovalent binding obtained from ITC (e.g., -23.4 kJ.mol^{-1}, see **SI, Fig. S9**), indicating that all 4 CRDs in DC-SIGN are engaged in Gx-psDiMan binding. This is also fully consistent with the DLS results described in the earlier section, where the saturated D_hs of Gx-psDiMan-DC-

Table 2. Summary of the standard binding thermodynamic parameters (T = 298 K) between Gx-psDiMan and DC-SIGN obtained *via* the GNP fluorescence quenching assay in comparison with the ΔH^0 values obtained by ITC. Errors represent the fitting errors.

Gx-psDiMan	GNP Fluorescence quenching assay			ITC
	ΔH^0 (kJ.mol^{-1})	ΔS^0 (J.K^{-1}.mol^{-1})	ΔG^0 (kJ.mol^{-1})	ΔH^0 (kJ.mol^{-1})
G5-psDiMan100%	-96.4 ± 2.6	-158 ± 9	-49.3 ± 2.7	-92.8 ± 1.6
G13-psDiMan100%	-93.0 ± 3.2	-125 ± 11	-55.7 ± 3.3	-99.9 ± 1.7

SIGN complexes match those expected for single Gx-psDiMan particles bound with a single layer of DC-SIGN molecules **(SI, Figs. S12 & S13**), indicating that DC-SIGN binds tetravalently using 4 CRDs to a single Gx-psDiMan.

ITC studies on DC-SIGN binding to Gx-psDiMan50% gave similar binding ΔH^0 values (e.g., -99.4 ± 2.7 and -93.6± 1.5 kJ/mol for x = 5 and 13, respectively, see **SI, Fig. S10**) to those of Gx-psDiMan100%, indicating the same tetravalent binding mode. These results are fully consistent with the glycan content dependent DC-SIGN binding affinity studies described in the earlier section (**Fig. 2, Table 1)**. Since the psDiMan contents in both Gx-psDiMan- 50% and 100% are higher than the minimal glycan density threshold, all 4 binding sites in each DC-SIGN molecule should be able to engage in binding with psDiMan groups from the same Gx-psDiMan particle to yield the maximal binding valency.

4. GNP-psDiMan inhibition of DC-SIGN-promoted EBOV$_{pp}$ cell entry.

To investigate whether the binding between DC-SIGN and Gx-psDiMan in solution faithfully replicates binding at the cell surface, we further investigated the ability of GNP-psDiMan to block DC-SIGN-promoted cellular entry of particles pseudotyped with the Ebola virus glycoprotein (EBOV$_{pp}$). The specific binding between DC-SIGN and the Ebola virus glycoprotein (EBOV-GP) promotes viral attachment and entry into host cells, which ultimately leads to infection. Binding of high affinity Gx-psDiMan to cell surface DC-SIGN should prevent binding of EBOV-GP to DC-SIGN, thereby blocking virus cellular entry and infection.[13-14, 21] Compared to other antiviral strategies, the use of entry inhibitors to block viral infection can be advantageous, since this can minimize virus developing resistance.[13-14, 21] Here, HEK293T cells transfected to express full length DC-SIGN and EBOV$_{pp}$ were employed to evaluate the antiviral properties of Gx-psDiMan (x = 5, 13) with 50% or 100% psDiMan content as described previously.[14, 20] The antiviral experiments were performed in DMEM medium supplemented with 10% feta bovine serum (FBS) as described previously.[14, 20] The raw inhibition data (luciferase activities) for each experiments together with negative controls were given in SI, **Fig. S14**. The normalized inhibition data (after correction of the background from control viral particles encoding no EBOV-GP gene) were fitted by a modified inhibition model as shown in eq. 6:[14, 48]

$$NI = 1/[1 + (C/EC_{50})^n] \qquad (6)$$

Where *NI*, *C*, EC_{50} and *n* are the normalized infection, Gx-psDiMan concentration, concentration giving 50% apparent inhibition, and inhibition coefficient (with *n* >, = and < 1 indicating positive-, non-, and negative- inhibiting cooperativity, respectively).[48] Whilst EC_{50} is a key indicator and widely used to assess the potency of antivirals, the inhibition coefficient "*n*" is much less mentioned in literature. However, "*n*" is also of great importance for antivirals: it indicates how quickly an inhibitor can achieve complete inhibition by increasing concentration. For example, three inhibitors have the same EC_{50} but different "*n*" values, the theoretical concentration required to inhibit 99% infection would be 9801, 99, and 9.9 times that of the EC_{50} value for *n* = 0.5, 1 and 2, respectively.[48] Therefore, antivirals displaying "*n*" ≥ 1 (with *n* = 1 being the most widely observed in literature) are much more effective inhibitors than those having *n* < 1, allowing for complete inhibition to be achieved at reasonable concentrations.

As shown in **Table 3,** both G5- and G13- psDiMan50% and 100% potently blocked cell surface DC-SIGN-promoted cell entry of EBOV$_{pp}$. Their EC_{50} values were determined as 0.43 ± 0.17, 0.06 ± 0.03, 0.49 ± 0.13 and 0.18 ± 0.04 nM, respectively. Such impressively low EC_{50} values place them among

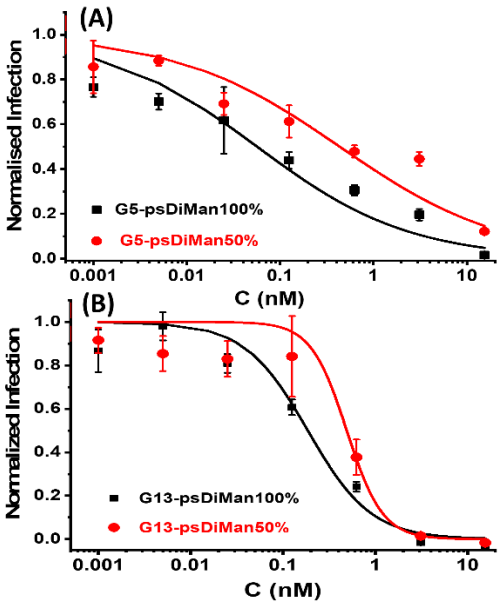

Fig. 5. Normalized infection (after background correction of the control particle encoding no EBOV-GP gene) *vs.* concentration plot for G5-psDiMan (**A**) or G13-psDiMan (**B**) against DC-SIGN augmented, EBOV-GP driven entry into HEK293 cells fitted by Eq. 6. The fitting parameters were provided in Table 3.

Table 3. Summary of the fitting parameters (EC_{50}, *n*, and R^2) for Gx-psDiMan inhibition of DC-SIGN-augmented cell entry of virus particles pseudotyped with EBOV-GP.

Gx-psDiMan	EC_{50} (nM)	n	R^2
G5-psDiMan50%	0.43 ± 0.17	0.49± 0.07	0.960
G5-psDiMan100%	0.06 ± 0.03	0.53± 0.09	0.915
G13-psDiMan50%	0.49 ± 0.13	2.2 ± 0.7	0.978
G13-psDiMan100%	0.18 ± 0.04	1.27± 0.26	0.981

the most potent glycoconjugate inhibitors against DC-SIGN-augmented cell entry of $EBOV_{pp}$.[2, 12, 14, 18, 20] Moreover, a higher surface psDiMan content (e.g., Gx-psDiMan50% *vs.* Gx-psDiMan 100%) was found to increase the antiviral potency of both G5- and G13- psDiMan. These results broadly agree with their relative DC-SIGN binding affinities measured in solution by GNP based fluorescence quenching. Interestingly, both G5-psDiMan50% and 100% displayed negative inhibition cooperativity (n = ~0.5) while their G13 counterparts appeared to exhibit no or even positive cooperativity ($n \geq 1$, after considering their relatively large fitting errors). Thus, a lower EC_{50} value for G5-psDiMan100% compared to that for G13-psDiMan100% (*e.g.,* 0.06± 0.03 *vs.* 0.18 ± 0.04 nM) does not necessarily mean that the former is a more effective antiviral than the latter. In fact, 3 nM G13-psDiMan100% completely blocked DC-SIGN-promoted $EBOV_{pp}$ cell entry (luciferase activity ≤ background signal of the control particle encoding no EBOV-GP gene), while its G5- counterpart only blocked ~80% of viral entry under the same concentration. The same trend was also observed for G5- and G13- psDiMan50%. This result highlighted the importance of "*n*" in determining the efficiency of antivirals: where both EC_{50} and "*n*" values much be considered together to obtain the true efficacy of antivirals. Further, it indicates that a large scaffold size is beneficial to antiviral properties of glycoconjugates based entry inhibitors.[18] Interestingly, the antiviral property of G5-psDiMan is different from that of G5-DiMan (G5 coated with LA-EG_2-EG_2-DiMan, a natural DiMan ligand for DC-SIGN with the same overall EG linker length). The former inhibition displayed negative cooperativity (n = ~0.5) while the latter displayed non cooperativity (n = 1).[14] Such differences are likely due to the different binding motifs between DiMan and psDiMan in binding to DC-SIGN CRDs. Crystal structures of psDiMan-DC-SIGN CRD complex revealed that psDiMan uses specific binding to the primary Ca^{2+} site *via* its mannose residue and the cyclohexane framework of the modified mannose form multiple contacts with Val351.[36] The restricted binding mode for psDiMan thus may require it to be presented at a specific orientation in order to maximize its binding contacts with DC-SIGN CRD. Whereas DiMan can coordinate the Ca^{2+} site with both Man residues, resulting in multiple binding modes which makes it more adaptable to CRD orientation. [37, 60] Since each LA based dithiol ligand forms 2 Au-S bonds on the GNP surface with an estimated total bonding enthalpy of ~90 kcal.mol^{-1}, matching that of a typical single C-C covalent bond.[14, 53] As a result, the psDiMan ligands on the GNP surface should not be mobile, apart from the flexibility offered by the EG_4 linker. Here, the EG_4 linker may not be able to provide enough flexibility to fully compensate the psDiMan orientation on curved GNP surfaces, allowing us to observe the different viral inhibition properties between G5-psDiMan and G5-DiMan.

Conclusion

In summary, by exploiting the versatile gold-thiol chemistry, tunable size, and powerful fluorescence quenching properties of GNPs,[40-42] we have developed the glycomimetic functionalized gold nanoparticles, Gx-psDiMan, as a powerful new biophysical probe for MLGIs. We have observed that the minimal psDiMan content threshold on GNP surface to form strong MLGI with DC-SIGN in solution is dependent upon the GNP scaffold size, which can be rationalized by the CRD's footprint. We have developed a new GNP based fluorescence quenching method to quantify MLGI binding thermodynamics by combining temperature-dependent affinity measurement and Van't Hoff analysis. We have revealed that Gx-psDiMan-DC-SIGN binding is enthalpy driven, with a binding ΔH^0 of ~-95 kJ.mol^{-1}, ~four times that of psDiMan-DC-SIGN monovalent binding, implying that all four binding sites in each DC-SIGN are engaged in binding with Gx-psDiMan. Importantly, this binding ΔH^0 value matches well to that measured from ITC, thus verifying the credibility of our GNP based fluorescence quenching method in probing MLGI thermodynamics. We have further demonstrated that Gx-psDiMan can potently block cell surface DC-SIGN augmented EBOV-GP driven virus cellular entry with sub-nM to mid-pM level of EC_{50} values. Such low EC_{50} values place them among the most potent glycoconjugate inhibitors against DC-SIGN mediated virus entry into host cells.[12-14, 18, 20] Moreover, we have observed that GNP scaffold size is critical towards the antiviral properties of glycan-nanoparticles. The smaller G5-psDiMan shows negative inhibition cooperativity (n = ~0.5), but the larger G13-psDiMan exhibits positive inhibition cooperativity (n > 1). As a result, the latter has achieved complete inhibition at a lower concentration than the former, despite of a higher EC_{50} value (*i.e.,* 0.18 ± 0.04 *vs.* 0.06 ± 0.03 nM). This result highlights the critical role of inhibition coefficient "*n*" in determining the efficiency and viability of glycoconjugate based antiviral entry inhibitors.

Experimental Section

Ligand Synthesis and characterization.

LA-EG_n-C≡CH linker molecules (n = 2, and 4) were synthesized by the standard dicyclohexylcarbodiimide/4-N,N-dimethylaminopyridine mediated amide coupling between lipoic acid and H_2N-EG_m-C≡CH (purchased commercially) in dry CH_2Cl_2 in good yields, e.g. 72% for n = 2, and 85% for n = 4, as reported previously.[14, 48] psDiMan appending an α-

$(CH_2)_2$-N_3 linker in the pseudo-anomeric position (psDiMan-C_2-N_3) was synthesized as described previously.[49] The LA-EG_n-C≡CH linker was then coupled to 1 molar equivalent of psDiMan-$(CH_2)_2$-N_3 (for n = 4) or commercial HO-EG_2-N_3 (for n = 2) *via* the copper-catalyzed click reaction in the presence of catalytic amount of $CuSO_4$ (0.05 molar equivalent), sodium ascorbate (for reducing Cu^{2+} to Cu^{+}) and tris(benzyltriazolylmethyl)amine (for stabilizing the Cu^{+} catalyst),[12] using our established protocols.[14, 48] The crude products were purified by size exclusion chromatography *via* Biogel P2 column using 20 mM ammonium formate aqueous solution as an eluent, giving the desired LA-EG_4-psDiMan and LA-EG_2-EG_2-OH ligands in ~72% and ~85% yields, respectively. Their $^1H/^{13}C$ NMR and LC-MS spectra were shown in **SI**, **Figs. S1 and S2**.

LA-EG_4-psDiMan: ^1H NMR (D_2O, 500 MHz): δ = 8.14 (s, 1H, triazole-H), 4.97 (d, 1H, *J*=1.8 Hz), 4.73 (d, 2H, *J*=7.2 Hz), 4.66 (s, 1H), 4.03 – 3.94 (m, 3H), 3.91 – 3.85 (m, 2H), 3.81 (dd, 1H, *J*=9.1, 3.4 Hz), 3.76 – 3.70 (m, 10H), 3.70 (s, 6H), 3.70 – 3.69 (m, 3H), 3.69 – 3.65 (m, 2H), 3.65 – 3.51 (m, 5H), 3.39 (t, 2H, *J*=5.2 Hz), 3.28 – 3.15 (m, 2H), 2.86 (ddd, 1H, *J*=13.0, 11.5, 3.7 Hz), 2.54 – 2.40 (m, 2H), 2.26 (t, 2H, *J*=7.3 Hz), 2.10 – 1.92 (m, 3H), 1.75 (tdd, 2H, *J*=13.6, 4.8, 2.2 Hz), 1.69 – 1.57 (m, 3H), 1.53 – 1.46 (m, 1H), 1.42 (q, 2H, *J*=7.8 Hz) ppm. ^{13}C NMR (D_2O, 125 MHz): δ = 177.4, 177.1, 176.9 (3xC=O), 125.6, 98.5, 73.7, 73.4, 70.8, 70.4 (2), 69.7, 69.6 (2), 69.5, 69.4, 68.9, 66.7, 66.5, 63.1, 61.0, 56.5, 52.5, 50.5, 40.2, 38.9, 38.8, 38.7, 38.0, 35.4, 33.7, 27.8, 26.7, 26.5, 25.0, ppm. LC-MS: calculated *m/z* for $C_{37}H_{63}N_4O_{16}S_2$ $(M+H)^+$ 883.37; found 883.59.

LA-EG_2-EG_2-OH: ^1H NMR (D_2O, 500 MHz): δ = 8.01 (s, 1H, triazole-H), 4.62 (s, 2H), 4.57 (t, 2H, *J*=5.0 Hz), 3.91 (t, 2H, *J*=5.1 Hz), 3.66 – 3.63 (m, 2H), 3.63 – 3.56 (m, 7H), 3.56 – 3.51 (m, 4H), 3.48 – 3.46 (m, 2H), 3.30 (t, 2H, *J*=5.3 Hz), 3.27 (s, 1H), 3.18 – 3.06 (m, 2H), 2.39 (dq, 1H, *J*=12.3, 6.1 Hz), 2.16 (t, 2H, *J*=7.2 Hz), 1.89 (dq, 1H, *J*=13.6, 6.8 Hz), 1.64 (dtd, 1H, *J*=13.6, 7.9, 5.5 Hz), 1.57 – 1.47 (m, 3H), 1.31 (p, 2H, *J*=7.4 Hz) ppm. ^{13}C NMR (D_2O, 125 MHz): δ = 176.9 (C=O), 143.9, 125.5, 71.7, 69.7, 69.4, 69.3, 69.0, 68.9, 68.7, 63.1, 60.3, 56.5, 50.0, 40.2, 38.9, 38.0, 35.4, 33.7, 27.7, 25.0 ppm. LC-MS: calculated *m/z* for $C_{21}H_{39}N_4O_6S_2$ $(M+H)^+$ 507.23; found 507.04.

Preparation of Gx-psDiMan conjugates. 5 nm GNPs (G5s) were synthesized in house using citrate reduction of $HAuCl_4$ in the presence of a small amount of tannic acid by following a literature method.[52] 13 nm GNPs (G13s) were synthesized by the standard citrate reduction method as reported previously.[50] For G5-psDiMan conjugation, citrate stabilized G5 was pre-concentrated *via* centrifugation by 4000 rpm, 20 min using a 10 kDa MWCO filter. The concentrated G5 aqueous solution was then added to a ligand mixture of LA-EG_4-psDiMan and LA-EG_2-EG_2-OH (with LA-EG_4-psDiMan content varying from 100, 75, 50, 25, 12.5, 6.3 and 0%) under a fixed total ligand: G5 molar ratio of 1000:1 and incubated at room temperature for 48 h with shaking to make G5-psDiMan via self-assembly. Any unbound ligands were then removed by washing the G5-psDiMan conjugates with deionized water using a 10 kDa cut-off MWCO filter *via* centrifugation by 10,000 ×g, 5 min for 3 times. The washing and flow through liquids were collected and combined to determine the amount of unbound LA-EG_4-psDiMan ligand to calculate GNP surface glycan valency.[14]

For G13-psDiMan conjugation, citrate stabilized G13 was added to the mixed LA-EG_4-psDiMan and LA-EG_2-EG_2-OH ligands (varying ratios as above) under a fixed total ligand: G13 molar ratio of 3000: 1 in a glass vial. The mixture was sonicated for 2 min, then incubated for a further 48 h at room temperature to complete G13-psDiMan conjugation. After that, the G13-psDiMan conjugates were transferred to Eppendorf tubes pretreated by 0.2% Tween 20, centrifuged at 17000 g, 30 min and washed with deionized water 3 times. The supernatant and washing liquids were collected to measure the amount of unbound LA-EG4-psDiMan ligands to calculate their glycan valency. The Gx-psDiMan conjugates were dispersed in pure water and their concentrations were calculated from their SPR peak absorbance at ~515 and ~520 nm using a molar extinction coefficient of 6.3 x 10^6 $M^{-1}cm^{-1}$ and 2.32 x 10^8 $M^{-1}cm^{-1}$ for G5 and G13,[14] respectively.

Binding studies *via* GNP fluorescence quenching assay. To quantify the binding affinities between DC-SIGN and Gx-psDiMan of varying psDiMan content (0 - 100%), Atto-643 labeled DC-SIGN (varying concentrations) was mixed with 1 molar equivalent of Gx-psDiMan in a binding buffer (20 mM HEPES, 100 mM NaCl, 2 mM $CaCl_2$, pH 7.8) containing 1 mg/mL of BSA, and then incubated for 20 min at room temperature. The protein concentration ranged from 0.1, 0.2, 0.5, 1, 2, 4, 8 to 16 nM for x = 5, or 0.1, 0.2, 0.4, 0.8, 1.6, 3.2 to 6.4 nM for x = 13, respectively. Fluorescence emission spectra were recoded over a range of 650-800 nm using a fixed λ_{EX} of 630 nm. Fluorescence spectra of labeled DC-SIGN at the above concentrations without Gx-psDiMan were also recorded under the identical conditions. The fluorescence spectra from 650 to 800 nm were integrated and used to calculate the quenching efficiency (QE) at each concentration (*C*) using eq. 1. The obtained QE - *C* plots were fitted by the Hill's equation (eq. 2) to derive their apparent binding K_ds.

For binding thermodynamic studies, DC-SIGN binding K_ds with both G5- and G13- psDiMan conjugates were measured under three different temperatures using the same method as described above. Then, the obtained $\ln(K_d)$ values were plotted against (1/T) and fitted by the linear function to obtain the slope and intercept, which correspond to the $\Delta H^0/R$ and $-\Delta S^0/R$, respectively, for the DC-SIGN-Gx-psDiMan binding. The error bars represent the standing

Isothermal titration calorimetry (ITC) assay. Wild-type DC-SIGN was dialysed overnight against the binding buffer (20 mM HEPES, 100 mM NaCl, 2 mM $CaCl_2$, pH 7.8) at 4 °C. The post-dialysis buffer was stored at 4 °C for subsequent experiments, including preparation of all samples, control titrations, and rinsing the syringe and cell between each measurement.

For the monovalent psDiMan binding study, the psDiMan was dissolved in the binding buffer to obtain a final concentration of 50 mM. DC-SIGN was concentrated by centrifugal ultrafiltration (10 kDa MWCO filter), to obtain a final concentration of 15 μM. Isothermal titration calorimetry was performed using a MicroCal iTC200, with the psDiMan solution loaded into the syringe, and DC-SIGN loaded into the calorimeter cell. Titrations were conducted at 25 °C with an initial 0.5 μL injection, followed by nineteen 2 μL injections.

A control experiment involving titration of psDiMan into the binding buffer (Figure S9(B)) was also recorded to measure the heat of dilution, which was then subtracted from the psDiMan-DC-SIGN binding titration to obtain the binding enthalpy change between psDiMan and DC-SIGN as shown in Figure S9(A). The standard MicroCal one set of sites model was used for fitting the plot of enthalpy changes, during which N (number of binding sites) was fixed at 4 as there are 4 CRDs on each DC-SIGN. The following binding thermodynamic parameters were obtained: K_d = 1.1 ± 0.3 mM, ΔH^o = -23.4 ± 2.7 kJ mol^{-1}, ΔG^o = -17.0 kJ mol^{-1} and ΔS^o = -21.5 J K^{-1} mol^{-1}.

For the Gx-psDiMan binding studies, the G5-psDiMan (100% and 50%) buffer was exchanged 3 times with the post-dialysis binding buffer using a 10 kDa cut-off centrifugal concentrator to obtain a final concentration of 300 nM. The G13-psDiMan buffer was similarly exchanged with the post-dialysis buffer using a 30 kDa cut-off centrifugal concentrator to obtain a final concentration of 100 nM. The DC-SIGN concentration used here was 30 μM. The DC-SIGN solution was loaded into the syringe, and Gx-psDiMan solution was loaded into the calorimeter cell. A titration of DC-SIGN into buffer was performed as a control titration. Enthalpy changes of Gx-psDiMan binding to DC-SIGN were obtained by subtracting the average of the last 4-8 data points of the control titration which have similar heat changes to correct the effect of heat dilution. The titration curve was fitted with the same method described above to obtain ΔH^o values.

Virus Inhibition. The inhibition effects of Gx-psDiMan (50% and 100%) on 293T cell entry of particles pseudotyped with the Ebola virus glycoprotein ($EBOV_{pp}$) were assessed using our established procedures.[14, 20] Briefly, 293T cells seeded in 96-well plates were transfected with plasmids encoding DC-SIGN or control transfected with empty plasmid (pcDNA). The cells were washed at 16 h post transfection and further cultivated at 37 °C, 5% CO_2 in Dulbecco's modified eagle medium (DMEM) containing 10% fetal bovine serum (FBS). At 48 h post transfection, the cells were exposed to twice the final concentration of Gx-psDiMan inhibitor in OptiMEM-medium for 30 min in a total volume of 50 μL. Thereafter, the resulting cells were inoculated with 50 μL of preparations of vesicular stomatitis virus (VSV) vector particles encoding the luciferase gene and bearing either EBOV-GP (which can use DC-SIGN/R for augmentation of host cell entry) or the VSV glycoprotein (VSV-G), which cannot use DC-SIGN for augmentation of host cell entry). Under these conditions, binding of Gx-psDiMan particles to 293T cell surface DC-SIGN receptors can block EBOV-GP interactions with these lectin receptors, resulting in reduced transduction efficiency of the virus particles and hence reducing the cellular luciferase activity. At 16-20 h post infection luciferase activities in cell lysates were determined using a commercially available kit (PJK), following the manufacturer's instructions, as described in our previous publication.[14, 20]

ASSOCIATED CONTENT

Supporting Information.

Experimental details including materials and methods, the synthesis procedures for LA-EG_4-DiMan and LA-EG_2-EG_2-OH ligand and their $^1H/^{13}C$ NMR and LC-MS spectra, determination of glycan conjugation efficiency and valency, surface footprint calculation, protein production, labeling and HR-MS characterization, fluorescence spectra of GNP quenching assays, ITC data and the original data of viral inhibition studies. This material is available free of charge via the Internet at http://pubs.acs.org.

AUTHOR INFORMATION

Corresponding Author

Yuan Guo – School of Food Science & Nutrition, and Astbury Centre for Structural Molecular Biology, University of Leeds, Leeds LS2 9JT, United Kingdom.
ORCID: 0000-0003-4607-7356.
Email: y.guo@leeds.ac.uk

Dejian Zhou – School of Chemistry and Astbury Centre for Structural Molecular Biology, University of Leeds, Leeds LS2 9JT, United Kingdom.
ORCID: 0000-0003-3314-9242.
Email: d.zhou@leeds.ac.uk

Authors:

Xinyu Ning – School of Chemistry and Astbury Centre for Structural Molecular Biology, University of Leeds, Leeds LS2 9JT, United Kingdom

Darshita Budhadev – School of Chemistry and Astbury Centre for Structural Molecular Biology, University of Leeds, Leeds LS2 9JT, United Kingdom

Sara Pollastri - Dipartimento di Chimica, Universita` degli Studi di Milano, via Golgi 19, Milano, Italy.

Inga Nehlmeier – Infection Biology Unit, German Primate Center, Leibniz Institute for Primate Research, 37077 Göttingen, Germany.

Amy Kempf – Infection Biology Unit, German Primate Center, Leibniz Institute for Primate Research, 37077 Göttingen, Germany.

Iain Manfield – School of Molecular and Cellular Biology and Astbury Cenrte for Structural Molecular Biology, University of Leeds, Leeds LS2 9JT, U.K.

W Bruce Turnbull – School of Chemistry and Astbury Centre for Structural Molecular Biology, University of Leeds, Leeds LS2 9JT, United Kingdom.

Anna Bernadi – Dipartimento di Chimica, Universita` degli Studi di Milano, via Golgi 19, Milano, Italy.

Stefan Pöhlmann – Infection Biology Unit, German Primate Center-Leibniz Institute for Primate Research and Faculty of Biology and Psychology, University of Göttingen, Göttingen 37073, Germany.

Xin Li- Sphere Fluidics Ltd., Building One, Granta Centre, Granta Park, Great Abington, Cambridge, England, CB21 6AL, United Kingdom.

Author Contributions

‡These authors contributed equally to this work.

Conflicting Interests

There is no conflicting Interest to declare.

Funding Sources

This project was supported by a UK Biotechnology and Biological Science Research Council grant (grant number: BB/R007829/1, to D.Z., W.B.T. & Y.G.), a University of Leeds Engineering and Physical Sciences Research Council Industrial Case Studentship (with Sphere Fluidics Ltd, to X.N.) and by the NextGenerationEU-MUR PNRR Extended Partnership initiative on Emerging Infectious Diseases (Project no. PE00000007, INF-ACT). We also thank the Wellcome Trust for support for equipment used during the project (094232/Z/10/Z).

ACKNOWLEDGMENT

We thank Dr Nicole Hondow for help in collecting TEM images of the GNPs. This project was supported by a UK Biotechnology and Biological Science Research Council grant (grant number: BB/R007829/1, to D.Z., W.B.T. & Y.G.), a University of Leeds Engineering and Physical Sciences Research Council Industrial Case Studentship (with Sphere Fluidics Ltd, to X.N.) and by EU funding within the Next Generation EU-MUR PNRR Extended Partnership initiative on Emerging Infectious Diseases (Project no. PE00000007, INF-ACT). We also thank the Wellcome Trust (U.K.) for supporting equipment used in this project (062164/Z/00/Z). For the purpose of open access, the authors have applied a Creative Commons Attribution (CC BY) license to any Author Accepted Manuscript version arising from this submission.

ABBREVIATIONS

GNP, gold nanoparticle; DC-SIGN, Dendritic Cell-Specific Intercellular adhesion molecule-3-Grabbing Nonintegrin; DC-SIGNR, DC-SIGN related lectin found on endothelial cells; TLC, thin layer chromatography; HPLC, high performance liquid chromatography; NMR, nuclear magnetic resonance; MS, mass spectrometry; ITC, isothermal titration calorimetry; DLS, dynamic light scattering.

REFERENCES

1. Mammen, M.; Choi, S. K.; Whitesides, G. M., Polyvalent interactions in biological systems: implications for design and use of multivalent ligands and inhibitors. *Angew. Chem. Int. Ed.* **1998,** *37* (20), 2754-2794.
2. Bernardi, A.; Jiménez-Barbero, J.; Casnati, A.; De Castro, C.; Darbre, T.; Fieschi, F.; Finne, J.; Funken, H.; Jaeger, K. E.; Lahmann, M.; Lindhorst, T. K.; Marradi, M.; Messner, P.; Molinaro, A.; Murphy, P. V.; Nativi, C.; Oscarson, S.; Penadés, S.; Peri, F.; Pieters, R. J.; Renaudet, O.; Reymond, J. L.; Richichi, B.; Rojo, J.; Sansone, F.; Schäffer, C.; Turnbull, W. B.; Velasco-Torrijos, T.; Vidal, S.; Vincent, S.; Wennekes, T.; Zuilhof, H.; Imberty, A., Multivalent glycoconjugates as anti-pathogenic agents. *Chem. Soc. Rev.* **2013,** *42* (11), 4709-4727.
3. Bhatia, S.; Camacho, L. C.; Haag, R., Pathogen Inhibition by Multivalent Ligand Architectures. *J. Am. Chem. Soc.* **2016,** *138* (28), 8654-66.
4. Brown, G. D.; Willment, J. A.; Whitehead, L., C-type lectins in immunity and homeostasis. *Nat. Rev. Immunol.* **2018,** *18* (6), 374-389.
5. Geijtenbeek, T. B. H.; Gringhuis, S. I., Signalling through C-type lectin receptors: shaping immune responses. *Nat. Rev. Immunol.* **2009,** *9* (7), 465-479.
6. Prasanphanich, N. S.; Mickum, M. L.; Heimburg-Molinaro, J.; Cummings, R. D., Glycoconjugates in host-helminth interactions. *Front. Immunol.* **2013,** *4*, 240.
7. Crocker, P. R.; Paulson, J. C.; Varki, A., Siglecs and their roles in the immune system. *Nat. Rev. Immunol.* **2007,** *7* (4), 255-66.
8. Drickamer, K.; Taylor, M. E., Recent insights into structures and functions of C-type lectins in the immune system. *Curr. Opin. Struct. Biol.* **2015,** *34*, 26-34.
9. Van Breedam, W.; Pohlmann, S.; Favoreel, H. W.; de Groot, R. J.; Nauwynck, H. J., Bitter-sweet symphony: glycan-lectin interactions in virus biology. *FEMS Microbiol. Rev.* **2014,** *38* (4), 598-632.
10. van Kooyk, Y.; Geijtenbeek, T. B., DC-SIGN: escape mechanism for pathogens. *Nat. Rev. Immunol.* **2003,** *3* (9), 697-709.
11. Kitov, P. I.; Sadowska, J. M.; Mulvey, G.; Armstrong, G. D.; Ling, H.; Pannu, N. S.; Read, R. J.; Bundle, D. R., Shiga-like toxins are neutralized by tailored multivalent carbohydrate ligands. *Nature* **2000,** *403* (6770), 669-672.
12. Ribeiro-Viana, R.; Sánchez-Navarro, M.; Luczkowiak, J.; Koeppe, J. R.; Delgado, R.; Rojo, J.; Davis, B. G., Virus-like glycodendrinanoparticles displaying quasi-equivalent nested polyvalency upon glycoprotein platforms potently block viral infection. *Nat. Commun.* **2012,** *3* (1), 1303.
13. Illescas, B. M.; Rojo, J.; Delgado, R.; Martín, N., Multivalent glycosylated nanostructures to inhibit Ebola virus infection. *J. Am. Chem. Soc.* **2017,** *139* (17), 6018-6025.
14. Budhadev, D.; Poole, E.; Nehlmeier, I.; Liu, Y.; Hooper, J.; Kalverda, E.; Akshath, U. S.; Hondow, N.; Turnbull, W. B.; Pohlmann, S.; Guo, Y.; Zhou, D., Glycan-Gold Nanoparticles as Multifunctional Probes for Multivalent Lectin-Carbohydrate Binding: Implications for Blocking Virus Infection and Nanoparticle Assembly. *J. Am. Chem. Soc.* **2020,** *142* (42), 18022-18034.
15. Sattin, S.; Bernardi, A., Glycoconjugates and Glycomimetics as Microbial Anti-Adhesives. *Trends Biotechnol.* **2016,** *34* (6), 483-495.
16. Cecioni, S.; Imberty, A.; Vidal, S., Glycomimetics versus multivalent glycoconjugates for the design of high affinity lectin ligands. *Chem. Rev.* **2015,** *115* (1), 525-61.
17. Smith, B. A. H.; Bertozzi, C. R., The clinical impact of glycobiology: targeting selectins, Siglecs and mammalian glycans. *Nat. Rev. Drug. Discov.* **2021,** *20* (3), 217-243.
18. Muñoz, A.; Sigwalt, D.; Illescas, B. M.; Luczkowiak, J.; Rodríguez-Pérez, L.; Nierengarten, I.; Holler, M.; Remy, J. S.; Buffet, K.; Vincent, S. P.; Rojo, J.; Delgado, R.; Nierengarten, J. F.; Martín, N., Synthesis of giant globular multivalent glycofullerenes as potent inhibitors in a model of Ebola virus infection. *Nat. Chem.* **2016,** *8* (1), 50-57.
19. Muller, C.; Despras, G.; Lindhorst, T. K., Organizing multivalency in carbohydrate recognition. *Chem. Soc. Rev.* **2016,** *45* (11), 3275-302.

20. Guo, Y.; Nehlmeier, I.; Poole, E.; Sakonsinsiri, C.; Hondow, N.; Brown, A.; Li, Q.; Li, S.; Whitworth, J.; Li, Z.; Yu, A.; Brydson, R.; Turnbull, W. B.; Pohlmann, S.; Zhou, D., Dissecting Multivalent Lectin-Carbohydrate Recognition Using Polyvalent Multifunctional Glycan-Quantum Dots. *J. Am. Chem. Soc.* **2017,** *139* (34), 11833-11844.

21. Bachem, G.; Wamhoff, E. C.; Silberreis, K.; Kim, D.; Baukmann, H.; Fuchsberger, F.; Dernedde, J.; Rademacher, C.; Seitz, O., Rational Design of a DNA-Scaffolded High-Affinity Binder for Langerin. *Angew. Chem. Int. Ed.* **2020,** *59* (47), 21016-21022.

22. Ramos-Soriano, J.; Ghirardello, M.; Galan, M. C., Carbon-based glyco-nanoplatforms: towards the next generation of glycan-based multivalent probes. *Chem. Soc. Rev.* **2022,** *51* (24), 9960-9985.

23. Hooper, J.; Budhadev, D.; Fernandez Ainaga, D. L.; Hondow, N.; Zhou, D.; Guo, Y., Polyvalent Glycan Functionalized Quantum Nanorods as Mechanistic Probes for Shape-Selective Multivalent Lectin-Glycan Recognition. *ACS Appl. Nano Mater.* **2023,** *6* (6), 4201-4213.

24. Gallego, I.; Ramos-Soriano, J.; Mendez-Ardoy, A.; Cabrera-Gonzalez, J.; Lostale-Seijo, I.; Illescas, B. M.; Reina, J. J.; Martin, N.; Montenegro, J., A 3D Peptide/[60]Fullerene Hybrid for Multivalent Recognition. *Angew. Chem. Int. Ed.* **2022,** *61* (41), e202210043.

25. Branson, T. R.; McAllister, T. E.; Garcia-Hartjes, J.; Fascione, M. A.; Ross, J. F.; Warriner, S. L.; Wennekes, T.; Zuilhof, H.; Turnbull, W. B., A Protein-Based Pentavalent Inhibitor of the Cholera Toxin B-Subunit. *Angew. Chem. Int. Ed.* **2014,** *53* (32), 8323-8327.

26. Leusmann, S.; Menova, P.; Shanin, E.; Titz, A.; Rademacher, C., Glycomimetics for the inhibition and modulation of lectins. *Chem. Soc. Rev.* **2023,** *52* (11), 3663-3740.

27. Guo, Y.; Sakonsinsiri, C.; Nehlmeier, I.; Fascione, M. A.; Zhang, H.; Wang, W.; Pöhlmann, S.; Turnbull, W. B.; Zhou, D., Compact, polyvalent mannose quantum dots as sensitive, ratiometric FRET probes for multivalent protein–ligand interactions. *Angew. Chem. Int. Ed.* **2016,** *55* (15), 4738-4742.

28. Hooper, J.; Liu, Y.; Budhadev, D.; Ainaga, D. F.; Hondow, N.; Zhou, D.; Guo, Y., Polyvalent Glycan Quantum Dots as a Multifunctional Tool for Revealing Thermodynamic, Kinetic, and Structural Details of Multivalent Lectin-Glycan Interactions. *ACS Appl. Mater. Interfaces* **2022,** *14* (42), 47385-47396.

29. Porkolab, V.; Pifferi, C.; Sutkeviciute, I.; Ordanini, S.; Taouai, M.; Thepaut, M.; Vives, C.; Benazza, M.; Bernardi, A.; Renaudet, O.; Fieschi, F., Development of C-type lectin-oriented surfaces for high avidity glycoconjugates: towards mimicking multivalent interactions on the cell surface. *Org. Biomol. Chem.* **2020,** *18* (25), 4763-4772.

30. Dam, T. K.; Brewer, C. F., Multivalent lectin-carbohydrate interactions energetics and mechanisms of binding. *Adv. Carbohydr. Chem. Biochem.* **2010,** *63*, 139-64.

31. Turnbull, W. B.; Daranas, A. H., On the value of c: can low affinity systems be studied by isothermal titration calorimetry? *J. Am. Chem. Soc.* **2003,** *125* (48), 14859-66.

32. Rao, J.; Lahiri, J.; Isaacs, L.; Weis, R. M.; Whitesides, G. M., A trivalent system from vancomycin.D-ala-D-Ala with higher affinity than avidin.biotin. *Science* **1998,** *280* (5364), 708-11.

33. Velazquez-Campoy, A.; Freire, E., Isothermal titration calorimetry to determine association constants for high-affinity ligands. *Nat. Protoc.* **2006,** *1* (1), 186-91.

34. Geijtenbeek, T. B. H.; Kwon, D. S.; Torensma, R.; van Vliet, S. J.; van Duijnhoven, G. C. F.; Middel, J.; Cornelissen, I.; Nottet, H.; KewalRamani, V. N.; Littman, D. R.; Figdor, C. G.; van Kooyk, Y., DC-SIGN, a dendritic cell-specific HIV-1-binding protein that enhances trans-infection of T cells. *Cell* **2000,** *100* (5), 587-597.

35. Pöhlmann, S.; Soilleux, E. J.; Baribaud, F.; Leslie, G. J.; Morris, L. S.; Trowsdale, J.; Lee, B.; Coleman, N.; Doms, R. W., DC-SIGNR, a DC-SIGN homologue expressed in endothelial cells, binds to human and simian immunodeficiency viruses and activates infection in trans. *Proc. Natl. Acad. Sci. U. S. A.* **2001,** *98* (5), 2670-2675.

36. Thepaut, M.; Guzzi, C.; Sutkeviciute, I.; Sattin, S.; Ribeiro-Viana, R.; Varga, N.; Chabrol, E.; Rojo, J.; Bernardi, A.; Angulo, J.; Nieto, P. M.; Fieschi, F., Structure of a glycomimetic ligand in the carbohydrate recognition domain of C-type lectin DC-SIGN. Structural requirements for selectivity and ligand design. *J. Am. Chem. Soc.* **2013,** *135* (7), 2518-29.

37. Feinberg, H.; Mitchell, D. A.; Drickamer, K.; Weis, W. I., Structural basis for selective recognition of oligosaccharides by DC-SIGN and DC-SIGNR. *Science* **2001,** *294* (5549), 2163-6.

38. Guo, Y.; Feinberg, H.; Conroy, E.; Mitchell, D. A.; Alvarez, R.; Blixt, O.; Taylor, M. E.; Weis, W. I.; Drickamer, K., Structural basis for distinct ligand-binding and targeting properties of the receptors DC-SIGN and DC-SIGNR. *Nat. Struct. Mol. Biol.* **2004,** *11* (7), 591-598.

39. Tamburrini, A.; Colombo, C.; Bernardi, A., Design and synthesis of glycomimetics: Recent advances. *Med. Res. Rev.* **2020,** *40* (2), 495-531.

40. Dubertret, B.; Calame, M.; Libchaber, A. J., Single-mismatch detection using gold-quenched fluorescent oligonucleotides. *Nat. Biotech.* **2001,** *19* (4), 365-370.

41. Dulkeith, E.; Ringler, M.; Klar, T. A.; Feldmann, J.; Muñoz Javier, A.; Parak, W. J., Gold nanoparticles quench fluorescence by phase induced radiative rate suppression. *Nano Lett* **2005,** *5* (4), 585-9.

42. Jennings, T. L.; Singh, M. P.; Strouse, G. F., Fluorescent Lifetime Quenching near d = 1.5 nm Gold Nanoparticles: Probing NSET Validity. *J. Am. Chem. Soc.* **2006,** *128* (16), 5462-5467.

43. Song, S. P.; Liang, Z. Q.; Zhang, J.; Wang, L. H.; Li, G. X.; Fan, C. H., Gold-Nanoparticle-Based Multicolor Nanobeacons for Sequence-Specific DNA Analysis. *Angew. Chem. Int. Ed.* **2009,** *48* (46), 8670-8674.

44. Susumu, K.; Uyeda, H. T.; Medintz, I. L.; Pons, T.; Delehanty, J. B.; Mattoussi, H., Enhancing the Stability and Biological Functionalities of Quantum Dots via Compact Multifunctional Ligands. *J. Am. Chem. Soc.* **2007,** *129* (45), 13987-13996.

45. Prime, K. L.; Whitesides, G. M., ADSORPTION OF PROTEINS ONTO SURFACES CONTAINING END-ATTACHED OLIGO(ETHYLENE OXIDE) - A MODEL SYSTEM USING SELF-ASSEMBLED MONOLAYERS. *J. Am. Chem. Soc.* **1993,** *115* (23), 10714-10721.

46. Zhou, D. J.; Bruckbauer, A.; Abell, C.; Klenerman, D.; Kang, D. J., Fabrication of three-dimensional surface structures with highly fluorescent quantum dots by surface-templated layer-by-layer assembly. *Adv. Mater.* **2005,** *17* (10), 1243-+.

47. Zhou, D.; Bruckbauer, A.; Ying, L. M.; Abell, C.; Klenerman, D., Building three-dimensional surface biological assemblies on the nanometer scale. *Nano Lett.* **2003,** *3* (11), 1517-1520.

48. Budhadev, D.; Hooper, J.; Rocha, C.; Nehlmeier, I.; Kempf, A. M.; Hoffmann, M.; Krüger, N.; Zhou, D. J.; Pöhlmann, S.; Guo, Y., Polyvalent Nano-Lectin Potently Neutralizes SARS-CoV-2 by Targeting Glycans on the Viral Spike Protein. *JACS Au* **2023**.

49. Reina, J. J.; Sattin, S.; Invernizzi, D.; Mari, S.; Martínez-Prats, L.; Tabarani, G.; Fieschi, F.; Delgado, R.; Nieto, P. M.; Rojo, J.; Bernardi, A., 1,2-mannobioside mimic:: Synthesis, DC-SIGN interaction by NMR and docking, and antiviral activity. *ChemMedChem* **2007,** *2* (7), 1030-1036.

50. Song, L.; Guo, Y.; Roebuck, D.; Chen, C.; Yang, M.; Yang, Z. Q.; Sreedharan, S.; Glover, C.; Thomas, J. A.; Liu, D. S.; Guo, S. R.; Chen, R. J.; Zhout, D. J., Terminal PEGylated DNA-Gold Nanoparticle Conjugates Offering High Resistance to Nuclease Degradation and Efficient Intracellular Delivery of DNA Binding Agents. *ACS Appl. Mater. Interfaces* **2015,** *7* (33), 18707-18716.

51. Song, L.; Ho, V. H. B.; Chen, C.; Yang, Z. Q.; Liu, D. S.; Chen, R. J.; Zhou, D. J., Efficient, pH-Triggered Drug Delivery Using a pH-Responsive DNA-Conjugated Gold Nanoparticle. *Adv. Healthc. Mater.* **2013,** *2* (2), 275-280.

52. Piella, J.; Bastús, N. G.; Puntes, V., Size-Controlled Synthesis of Sub-10-nanometer Citrate-Stabilized Gold Nanoparticles and Related Optical Properties. *Chem. Mater.* **2016,** *28* (4), 1066-1075.

53. Zhao, Y. X.; Zhou, F.; Zhou, H. C.; Su, H. B., The structural and bonding evolution in cysteine-gold cluster complexes. *Phys. Chem. Chem. Phys.* **2013,** *15* (5), 1690-1698.

54. Saha, S. K.; Brewer, C. F., Determination of the concentrations of oligosaccharides, complex type carbohydrates, and glycoproteins using the phenol-sulfuric acid method. *Carbohydr. Res.* **1994,** *254*, 157-67.

55. Hill, H. D.; Millstone, J. E.; Banholzer, M. J.; Mirkin, C. A., The Role Radius of Curvature Plays in Thiolated Oligonucleotide Loading on Gold Nanoparticles. *Acs Nano* **2009,** *3* (2), 418-424.

56. Stewart-Jones, G. B. E.; Soto, C.; Lemmin, T.; Chuang, G.-Y.; Druz, A.; Kong, R.; Thomas, P. V.; Wagh, K.; Zhou, T.; Behrens, A.-J.; Bylund, T.; Choi, C. W.; Davison, J. R.; Georgiev, I. S.; Joyce, M. G.; Kwon, Y. D.; Pancera, M.; Taft, J.; Yang, Y.; Zhang, B.; Shivatare, S. S.; Shivatare, V. S.; Lee, C.-C. D.; Wu, C.-Y.; Bewley, C. A.; Burton, D. R.; Koff, W. C.; Connors, M.; Crispin, M.; Baxa, U.; Korber, B. T.; Wong, C.-H.; Mascola, J. R.; Kwong, P. D., Trimeric HIV-1-Env Structures Define Glycan Shields from Clades A, B, and G. *Cell* **2016,** *165* (4), 813-826.

57. Feinberg, H.; Guo, Y.; Mitchell, D. A.; Drickamer, K.; Weis, W. I., Extended neck regions stabilize tetramers of the receptors DC-SIGN and DC-SIGNR. *J. Biol. Chem.* **2005,** *280* (2), 1327-35.

58. Zhang, H. Y.; Feng, G. Q.; Guo, Y.; Zhou, D. J., Robust and specific ratiometric biosensing using a copper-free clicked quantum dot-DNA aptamer sensor. *Nanoscale* **2013,** *5* (21), 10307-10315.

59. Holla, A.; Skerra, A., Comparative analysis reveals selective recognition of glycans by the dendritic cell receptors DC-SIGN and Langerin. *Protein Eng. Des. Sel.* **2011,** *24* (9), 659-69.

60. Feinberg, H.; Castelli, R.; Drickamer, K.; Seeberger, P. H.; Weis, W. I., Multiple modes of binding enhance the affinity of DC-SIGN for high mannose N-linked glycans found on viral glycoproteins. *J. Biol. Chem.* **2007,** *282* (6), 4202-9.

TOC figure